 doi:10.20944/preprints201711.0001.v1

Article

Investigations on Corrosion Behaviors of Super-Strength Sucker Rod Steel in High SO_4^{2-} Environment

Zhongying Han [1], Xiaoguang Huang [2]*, Yinfeng Li [3]

1. School of Petroleum Engineering, China University of Petroleum(East China), Qingdao266580, China
2. Department of Engineering Mechanic, China University of Petroleum(East China), Qingdao266580, China
3. Department of Engineering Mechanics, Shanghai Jiao Tong University, Shanghai200240 China.
Email: huangxg@upc.edu.cn

Abstract

In some sour reservoirs and tertiary oil recovery blocks, SO_4^{2-} in solution can cause the corrosion and corrosion fatigue of the sucker rods. In this paper, the corrosion behaviors of super-strength sucker rod FG20 (16Mn2SiCrMoVTiA) steel in the well fluid are investigated by electrochemical measurements, and electron probe micro-analyzer (EPMA) analysis. The results show that FG20 steel has a favorable corrosion resistance in neural solutions. When the hydrogen ion content increases, the hydrolysis of SO_4^{2-} greatly accelerates the corrosion of FG20 steel. The energy dispersive X-ray(EDX)results demonstrate that the corrosion process of FG20 steel in neural well liquid is an oxygen concentration process, and the protective $FeCO_3$ and Fe_2O_3 on the surface of the samples can prevent further corrosion. With the increase of the acidity in the well liquid, the corrosion process converts into a sulphide concentration process, and the sloppy FeS and mackinawite film cannot provide effective protection for the specimens, resulting in the increase of corrosion rate.

Key words: corrosion behavior; FG20; electrochemical measurements; EPMA; corrosion mechanism

1. Introduction

A comprehensive view of the world oil-gas development process indicates that rod-having pump oil-production is the most traditional and most widely used method[1]. Approximately 75% of China's oil production has been obtained by the sucker rod pumping technology. As the number of deep and ultra-deep wells increases, the pump depth and rod load of sucker rods increase accordingly. Meanwhile, due to the tertiary oil recovery, especially the applications of sewage treatment and reinjection, the service environment of the sucker rod is worsening [2-4]. High salinity and high corrosivity of well fluid aggravate the corrosion of sucker rods[5-6]. The conventional Chinese D and E grade sucker rods can no longer meet the needs of the exploitation of unconventional reservoirs [7]. Hence, to develop sucker rods with super performance is imperative formost oilfields.

FG20 steel is a new material for super strength sucker rodsmade in China. It is a typical bainite steel containing Cr, Mn, and Mo elements that can promote the formation of bainite to ensure that the structures have the right amount of residual austenite in air cooling conditions. At the same time, through the grain refinement strengthening of vanadium and precipitation strengthening of titanium, the vanadium titanium micro alloying process ensures that the steel has good strength and toughness. FG20 steel has been made and developed since the 1990s, and now has been popularized and applied. However, the papers on the performance of FG20 steel in the environment of high salinity and high corrosivity are rarely found. And the studies related to the service life prolongation of FG20 steel compared with the conventional E and D grade sucker rods have little been reported.

In the present work, the corrosion behaviors of FG20 steel in the well fluid are studied, and the effects of fluid pH on the corrosion rates, Tafel polarization and electrochemical impedance spectroscopy (EIS) are investigated. Electron probe micro-analyzer (EPMA) analysis is used to analyze the corrosion mechanism of FG20 steel.

Preprints (www.preprints.org) | NOT PEER-REVIEWED | Posted: 1 November 2017 doi:10.20944/preprints201711.0001.v1

2. Material and test methods

2.1. Material and specimen

The specimen of super-strength sucker rod steel FG20 for electrochemical test comes from controlled rolling plates(17.6mm thick) manufactured by Tangshan Steel. The chemical compositions(mass %) are as follows: 0.17%C, 0.015%Ni, 0.68%Si, 0.21%Mn, 0.58%Cr, 0.042%V, 0.23%Mo, 0.017%P, 0.019%S, 0.051%Ti, and Fe rem. The mechanical properties are shown in Table 1.

Table 1 Mechanical properties of FG20 steel

σ_s/MPa	σ_b/MPa	δ/%	ψ/%	Fatigue strength $\sigma_{0.1}$/MPa
832	1036	17.4	48	550(cycles>10^6)

2.2. Electrolyte solution preparation

The corrosive well fluid was taken from the GO7-32-375 stratum of Gudong Oil Plant, Shengli Oil Field. Gudong Plant is a typical tertiary oil region in Shengli Oil Field. High salinity and remarkable changes in temperature, pressure and pH are the characteristics of the underlying liquid. The corrosion behaviors of sucker rods in this reservoir are very complex, and the corrosion mechanism of FG20 sucker rod in different blocks is different. The depth of GO7-32-375 stratum is about 1200 meter, and the well water temperature is about 60°C. The chemical compositions of the solution are listed in Table 2. To analyze the effect of pH on corrosion behavior of FG20 steel in the well fluid, the dilute hydrochloric acid (5 wt%) was used to modulate the pH of the well liquid.

Table 2 Chemical compositions (mg/L) of the selected well liquid

composition	oil fraction	SO_4^{-2}	O_2	CO_2	Cl^-	total salinity	pH
content	63.7	724.98	0.02	0.043	1160.35	6165.24	6.8

2.3. Tafel polarization and EIS measurement

The electrochemical measurements were performed in a Perkin-Elmer M283 constant potential electrochemical testing system using a three- electrode cell, where a saturated calomel electrode (SCE) was used as the reference electrode and a platinum sheet as the counter electrode. The FG20 specimen is used as the working electrode, and its size is shown in Fig.1. The specimens were progressively grinded by a series of water sandpapers, and finally polished by a 5μm diamond paste. Before the tests, all the specimens were successively rinsed with deionized water and acetone, and then dried.

All the electrochemical tests were conducted at 60±1°C. To maintain the experimental temperature, a specific water bath container was used as shown in Fig.2. The specimens were immersed in the well fluid at an open-circuit potential (OCP) for 1 hour prior to the Tafel polarization measurement. Cyclic potentiodynamic polarization measurements were conducted starting from -250mV (vs open circuit potential), and scanned toward more positive direction with the scanning rate of 0.5mV/s. When the current reached 1 mA, the scanning direction was reversed. EIS measurements were conducted at OCP with a sinusoidal perturbation of 10 mV amplitude at measurement frequency ranging from100 kHz-100 mHz, aided by the M1025 frequency response instrument. The data was acquired in four cycles at each frequency to provide good precision at all frequencies. All the test data was analyzed by SofrCorr III based on the nonlinear least-square algorithm. For better reproducibility, all aforementioned electrochemical experiments were repeated more than three times.

Preprints (www.preprints.org) | NOT PEER-REVIEWED | Posted: 1 November 2017 doi:10.20944/preprints201711.0001.v1

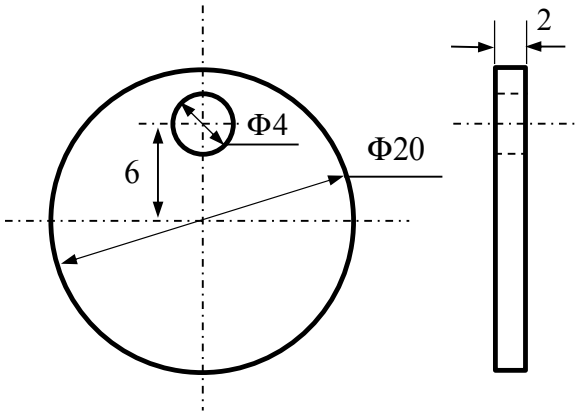

Fig.1 The dimensions of specimen

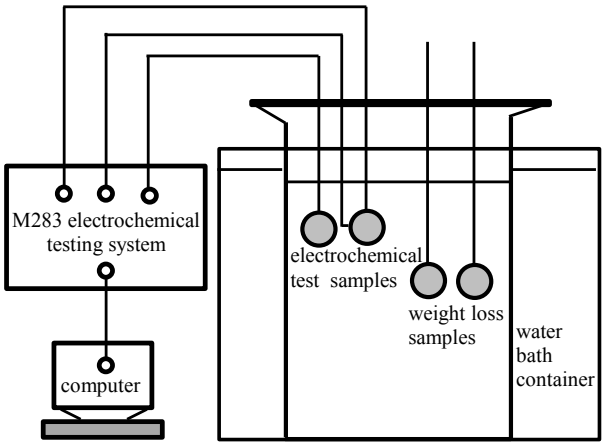

Fig.2 Schematic of the test bench

2.4. Weight loss test

Specimens for weight loss tests (WLT) are the same as that for electrochemical measurements and three samples used for each series were measured for good reproducibility. The test temperature was maintained at 60±1°C by a temperature control unit, and the solution was replaced weekly. Before the test, the specimens were successively washed by acetone and absolute ethanol and dried, and then weighed by a digital balance with an accuracy of 0.00001g for the original weight(W_0) before immersed in the test solutions. After being immersed for 30 days and 90 days, the corroded specimens were taken out from the solutions. The corrosion products on specimen surfaces were removed using a special chemical products-cleanup liquid. Finally, the samples were weighed again to obtain the final weight (W_1). The corrosion rates of the samples are calculated by Eq. (1)[8]:

$$V_{corr} = \frac{8.76\times10^4\times(W_1 - W_0)}{\rho A t} \quad (1)$$

where V_{corr} is the corrosion rate(mm/a), W_0 and W_1 are the original weight and final weight of specimens(g), respectively, ρ is the mass density(g/cm^3), A is the exposed surface area of specimens(cm^2), and t is the immersion time(s).

Preprints (www.preprints.org) | NOT PEER-REVIEWED | Posted: 1 November 2017 doi:10.20944/preprints201711.0001.v1

After the weight loss test, the corrosion morphology and surface features of some corroded FG20 samples were observed by JXA-8230 EPMA, and the energy spectrum of corrosion products were analyzed to determine the corrosion mechanism in the different well fluids.

3. Results and discussions

3.1. Tafel polarization curves

The Tafel polarization curves of FG20 samples in the corrosive liquids with different pH are shown in Fig.3. It can be seen that the polarization curves remarkably accelerates with the pH decrease in the solution. With the decrease of the solution pH, the self-corrosion potential increases, the polarization curve shifts to the right, the current density increases, and the corrosion rate increases. Meanwhile, the anode Tafel slope declines with the decline of pH. The anodic reaction is inhibited because the corrosion at electrode surface is more serious and the formation of sulfide film effectively reduces the effective area of electrode corrosion, and then blocks the chemical reaction effect on the electrode surface. The cathode Tafel slope goes up and the corrosion potential becomes higher with the decline of pH. At the same time, the cathodic depolarization becomes stronger, and the electrode reaction is intense and controlled by hydrogen evolution. However, the corrosion products on the electrode surface have poor compactness and adhesion, and no actually protective effect, resulting in accelerated corrosion of FG20 samples.

The electrochemical parameters obtained from the polarization curve analysis provide more details about the overall corrosion process. According to the four-point method for determining the corrosion rate developed by Jankowski et. al. [9]and Tang[10], the corrosion current density (I_{corr}), Tafel constant(b_a and b_c represent anodic and cathodic, respectively) and polarization resistance (R_p)are determined and shown in Table 3.

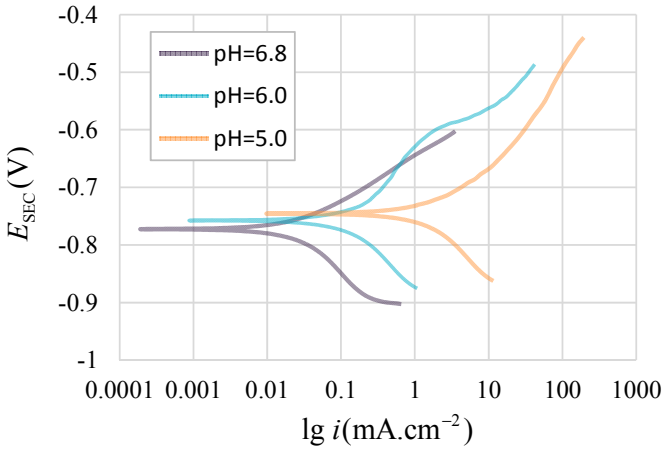

Fig.3 Potentiodynamic polarization curves of FG20 steel in different well fluids

Table 3 The electrochemical parameters from polarization curve analysis in different solutions

pH	E_{corr}(V)	I_{corr}(mA·cm^{-2})	b_a(V·dec^{-1})	b_c(V·dec^{-1})	R_P^*(Ωcm^2)
6.8	-0.772	0.013	0.056	0.204	1469.514
6.0	-0.758	0.041	0.069	0.158	509.294
5.0	-0.742	0.148	0.087	0.129	152.639

*Polarization resistance (R_p) is calculated by the following equation: $R_p = \frac{b_a b_c}{2.3 I_{corr}(b_a + b_c)}$ [10]

3.2. EIS measurement

The Nyquist plots of FG20 samples in the solutions with different pH are shown in Fig.4. Each curve contains one semi-circle, representing the Faraday resistance of the interface between the metal electrode and the solution. The shape and the diameter of the experimental impedance circle depend

Preprints (www.preprints.org) | NOT PEER-REVIEWED | Posted: 1 November 2017 doi:10.20944/preprints201711.0001.v1

on the pH of the well fluids. The lower the pH, the smaller the diameter of the impedance circle. If the equivalent circuit of the corrosion system shown in Fig.3 is adopted, where R_1 is the solution resistance between the working electrode and Luggin capillary, Q is the constant phase element whose behavior is attributed to the surface roughness and heterogeneities, electrode porosity, etc.; and R_2 is the reaction resistance at the interface between the solid electrode and well fluid[11-13]. The equivalent circuit parameters in the well fluids are listed in Table 4. It can be seen from the table that $R_1$and R_2 both decrease with the decline of pH, while Q varies inversely. The reaction resistance at the interface R_2 reflects the surface activity and corrosion resistance of the specimen. The smaller the R_2, the worse the corrosion resistance and the higher surface activity. Consequently, the increasing acidity of the well fluid increases the corrosion current density, and accelerates the electrochemistry corrosion of FG20 steel.

The Bode plots of FG20 samples in different solutions are depicted in Fig. 5. With the pH decrease, the frequency corresponding to the phase angle peak changes slightly, but the phase angle increases obviously. These features demonstrate that the capacitance between the electrode and solution increases and the charge transfer resistance decreases gradually, leading to the acceleration of the corrosion. The results of EIS are consistent with those of Tafel polarization tests.

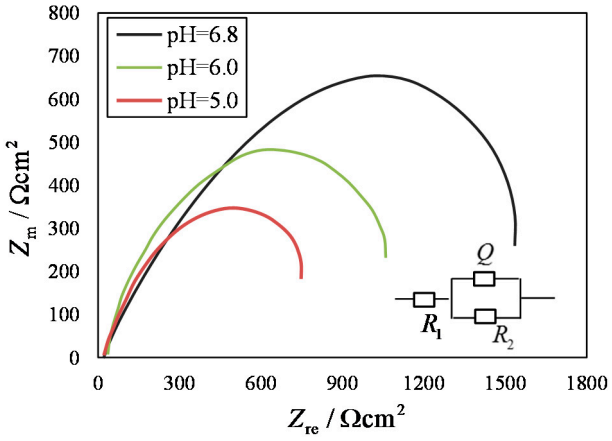

Fig.4 Nyquist plots of FG20 steel in different solutions

Table 4 The equivalent circuit parameters in different solutions

pH	$R_1(\Omega)$	Q	$R_2(\Omega)$
6.8	2.11	5.31×10^{-5}	8.94×10^{5}
6.0	1.43	8.82×10^{-5}	1.43×10^{5}
5.0	0.45	1.14×10^{-4}	3.78×10^{4}

Preprints (www.preprints.org) | NOT PEER-REVIEWED | Posted: 1 November 2017 doi:10.20944/preprints201711.0001.v1

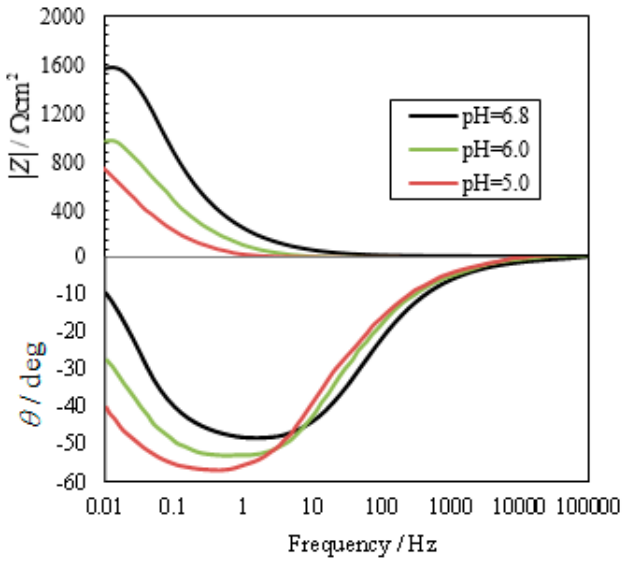

Fig.5 Bode plots of FG20 steel in solutions with different pH

3.3. Corrosion rates

After removing the corrosion products on the WLT specimens, the corrosion rates of FG20 steel in the well fluids were calculated by Equation (1) and listed in Table 5. The corrosion rate of FG20 steel increases significantly with decreasing pH in the well fluid. The corrosion rate increases up to 0.914mm/a in the pH=5.0 solution, which is nearly 6 times greater than that in the nearly neutral well fluid (pH=6.8). The results indicate that the pH in the well fluid has a strong impact on the corrosion resistance of the FG20 steel, and the material shows a greater activity with the increase of acidity in the solution. The corrosion rates in the 90 day period were also calculated and presented in Fig.6 for comparison. It indicates that the results of the two test periods are in good agreement, and the weight loss results of the 30-day test are credible.

Table5 Corrosion rates of FG20 steel (test period: 30 day)

pH	SP No.	W_0(g)	W_1(g)	ΔW(g)	V_{corr}(mm/a)
6.8	1#	4.694	4.625	0.069	0.143
	2#	4.721	4.650	0.071	0.147
	3#	4.679	4.614	0.065	0.135
	aver	4.698	4.630	0.068	0.142
6.0	4#	4.715	4.509	0.206	0.426
	5#	4.724	4.527	0.197	0.407
	6#	4.717	4.523	0.194	0.401
	aver	4.719	4.520	0.199	0.411
5.0	7#	4.745	4.297	0.448	0.925
	8#	4.695	4.258	0.437	0.902
	9#	4.710	4.267	0.443	0.915
	aver	4.717	4.274	0.443	0.914

Preprints (www.preprints.org) | NOT PEER-REVIEWED | Posted: 1 November 2017 doi:10.20944/preprints201711.0001.v1

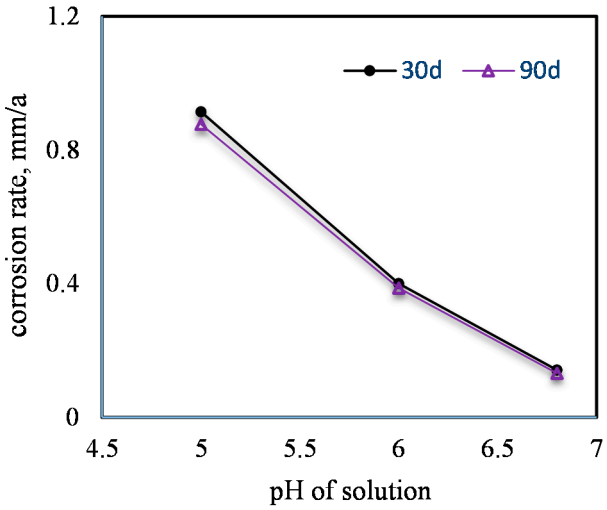

Fig.6 Comparison of corrosion rates in different test periods

3.4. Energy spectrum and corrosion mechanism

To study corrosion mechanism of FG20 steel in the well fluid and analyze the effect of pH on the corrosion mechanism, secondary electron images (SEI) of corroded surfaces were observed after weight loss tests. The SEI and EDX photographs are shown in Fig.7. It can be seen that the corrosion morphology of the corroded sample is significantly dependent on the pH in the well fluid. In the pH=5.0 solution, the corrosion product films are loose in structure and have deep cracks, as shown in Fig. 7 (a). The corrosion products mainly contain Fe and S elements, and also contain a very small amount of O element, as illustrated in Fig. 7 (b). To obtain the overall composition of corrosion products and overcome the shortage of one-point analysis in Fig.7(a), and region analysis was adopted and the results are presented in Fig.8. The total corrosion products in the region marked by the red box in Picture (a) were analyzed and the main elements were evaluated and listed in the right-hand table, and the main chromatograms of chemical elements in this region are shown in pictures from (b) to (i), respectively. Both the point and region analysis indicate that the corrosion products are mainly composed of FeS or mackinawite FeS_{1-x} [14-15], and a small amount of $Fe(OH)_2$ or Fe_2O_3. This corrosion process can be considered as the sulphide concentration process [16], and is dominated by the following reactions:

$$\text{Cathode:}\quad SO_4^{2-}+9H^++8e^- \rightarrow HS^- + 4H_2O$$

$$Fe+2H_2O \rightarrow Fe(OH)_2+2e^- + 2H^+$$

$$\text{Anode:}\quad Fe(OH)_2+HS^- \rightarrow FeS+OH^- + 2H_2O$$

The FeS film cannot form an effective protective layer on the surface, which easily results in pitting corrosion on the surface of the samples[17]. However, with the pH increase in the solution, the corrosion behavior at the surface of the sample is restrained compared with that in pH=5.0 solution. S content decreases, and O and C contents increase in the corrosion products, as shown in Fig.6(d) and (f). The figures demonstrate that the FeS content decrease and the protective $FeCO_3$ and gradual Fe_2O_3 increase result in the decrease of the corrosion rate. This process can be considered as an oxygen concentration process, and the reactions are dominated by:

$$\text{Cathode:}\quad CO_2+H_2O \rightarrow H_2CO_3$$

$$H_2CO_3 \rightarrow H^+ + HCO_3^-$$

$$HCO_3^- \rightarrow H^+ + CO_3^{2-}$$

$$\text{Anode:}\quad Fe+2H_2O \rightarrow Fe(OH)_2+2e^- + 2H^+$$

Preprints (www.preprints.org) | NOT PEER-REVIEWED | Posted: 1 November 2017 doi:10.20944/preprints201711.0001.v1

200 $$Fe(OH)_2 + CO_2 \rightarrow FeCO_3 + H_2O$$

201 $$4Fe(OH)_2 + O_2 \rightarrow 2Fe_2O_3 + 4H_2O$$

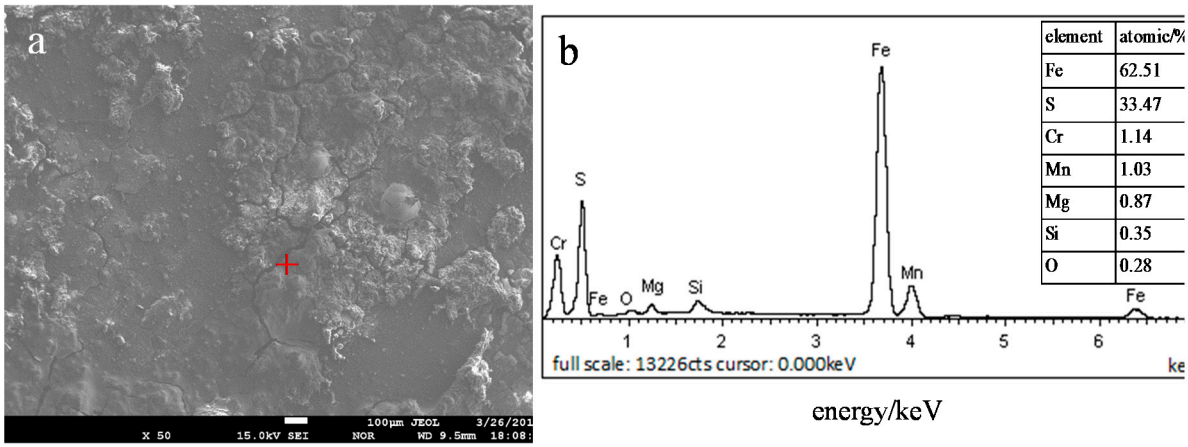

a b

202

203

204 (a) SEI micrograph of FG20 in the pH=5.0 well fluid (b) EDX analysis of FG20 in the
205 pH=5.0 well fluid

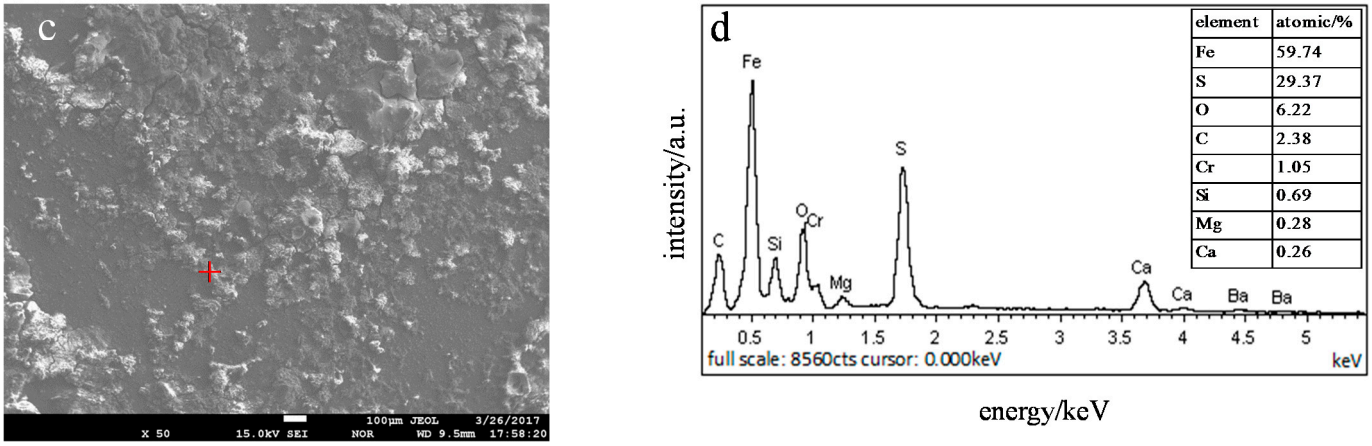

c d

206 (c) SEI micrograph of FG20 in the pH=6.0 well fluid (d) EDX analysis of FG20 in the
207 pH=6.0 well fluid

Preprints (www.preprints.org) | NOT PEER-REVIEWED | Posted: 1 November 2017 doi:10.20944/preprints201711.0001.v1

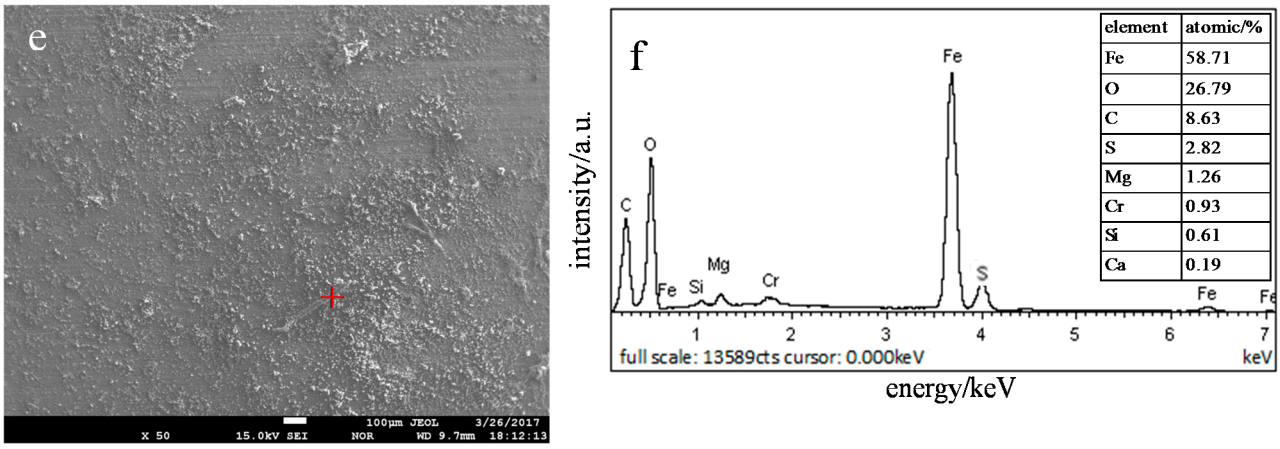

e f

208

209 (e) SEI micrograph of FG20 in the pH=6.8 well fluid (f) EDX analysis of FG20 in the
210 pH=6.8 well fluid

211 **Fig.**7 SEI micrograph and EDX analysis of FG20 in the well fluid

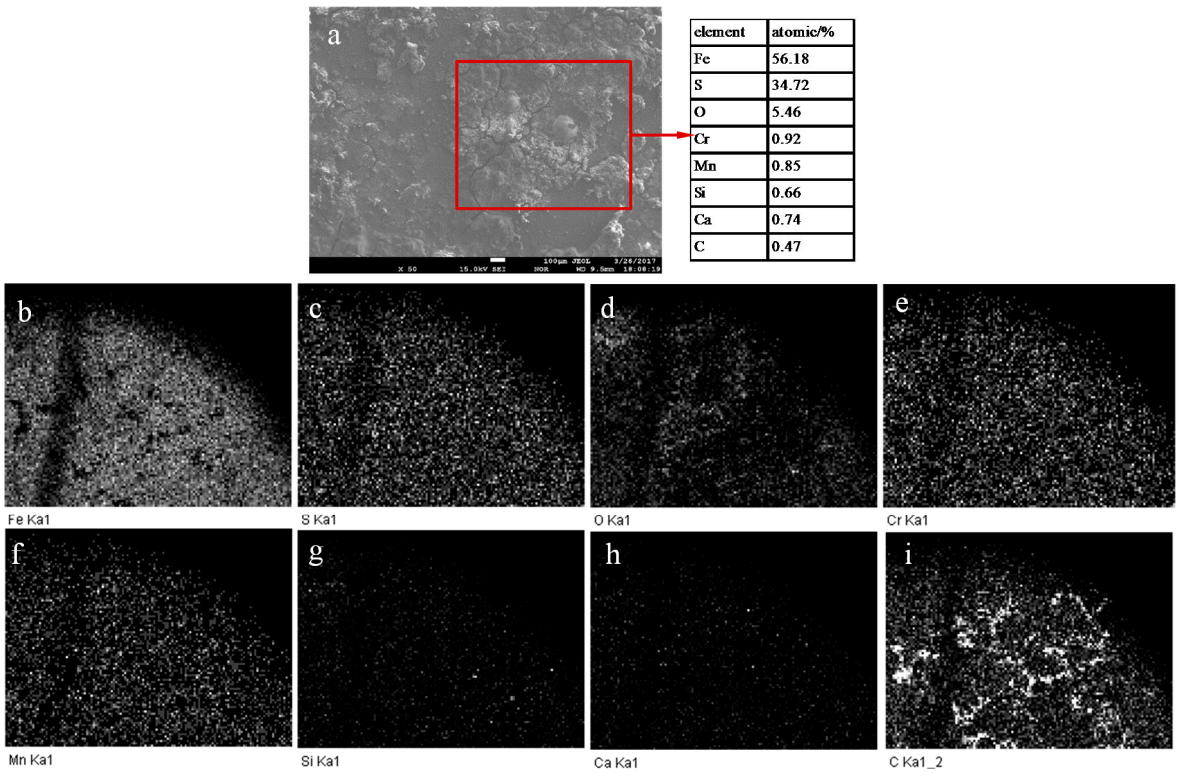

212

213 **Fig.**8 Chemical compositions and contents of corrosion products in pH=5.0 solution

214 **4. Conclusions**

215 (1) In high SO_4^{2-} and Cl^- well liquid, corrosion resistance of FG20 steel is good in a neural
216 solution; however the corrosion rate accelerates with the pH decrease of solution.
217 (2) As the solution pH decreases, corrosion potential becomes more negative, polarization
218 resistance falls quickly, and polarization current density increases continually. Low pH aggravates

 doi:10.20944/preprints201711.0001.v1

both cathodic and anodic reactions of FG20 steel, leading to more serious corrosion on the sample surface.

Because of the enrichment of SO_4^{2-}, the concentration of hydrogen ions in solution dominates the corrosion mechanism of FG20 to a great extent. The enriched hydrogen ions accelerate the hydrolysis of SO_4^{2-}, and generate FeS or mackinawite FeS_{1-x} film on the surface of the samples. FeS or FeS_{1-x} film cannot prevent the further corrosion of the samples. Nevertheless, with the solution pH increase, hydrolysis of SO_4^{2-} decreases, and the oxygen concentration process gradually dominates the corrosion process. The dense corrosion products, $FeCO_3$ and Fe_2O_3, can effectively reduce the reaction between FG20 and the corrosive solution, resulting in the decrease of corrosion rate.

Acknowledgments

The research is supported by the Fundamental Research Funds for the Central Universities of China (No.17CX02065), and the Natural Science Foundation of China (No.51404286).

References

[1] G. Takacs. Sucker-rod pumping system components and their operation(chapter 3)[M]. Elsevier: Sucker-rod pumping handbook, 2015: 57–246.

[2] Y. Sugaia, K. Sasakia,R. Wakizonoa, Y. Higuchib,N. Muraoka. Considerations on the possibility of microbial clogging of re-injection wells of the wastewater generated in a water-dissolved natural gas field[J]. International Biodeterioration & Biodegradation, 2013, 81(1): 35–43.

[3] M. Tagliabuea , A.P. Reverberib, R. Bagatina. Boron removal from water: needs, challenges and perspectives[J]. Journal of Cleaner Production, 2014, 77(77): 56–64.

[4] P. Jain, M. Sharma, P. Dureja, P.M. Sarma, B. Lal. Bioelectrochemical approaches for removal of sulfate, hydrocarbon and salinity from produced water[J]. Chemosphere, 2017, 166: 96–108.

[5] A. Hedayat, S. Yannacopoulos, J. Postlethwaite. Wear and CO_2 corrosion of steel couplings and tubing in heavy oil screw-pump wells[J]. Wear, 1997, 209(1-2): 263–273.

[6] Z.Y. Hu, D.L. Duan , S.H. Hou, X.J. Ding, S. Li. Preliminary Study on Corrosion Behaviour of Carbon Steel in Oil–Water Two-Phase Fluids[J]. Journal of Materials Science & Technology, 2015, 31(12): 1274–1281.

[7] D.L. Duan, Z. Geng, S.L. Jiang , S. Li. Failure mechanism of sucker rod coupling[J].Engineering Failure Analysis, 2014, 36: 166–172.

[8] J.H. Ding, L. Zhang, D.P. Li, M.X. Lu, J.P. Xue, W. Zhong. Corrosion and stress corrosion cracking behavior of 316L austenitic steel in high H2s-CO2-Cl-environment[J]. Journal of Materials Science, 2013, 48(10):3708–3715.

[9] J. Jankowski, R. Juchniewicz. A four-point method for corrosion rate determination[J].

255 Corrosion Science, 1980, 20(7): 841–851.
256 [10] J.W. Tang, Y.W. Shao, T. Zhang, G.Z. Meng, F.H. Wang. Corrosion behaviour of carbon
257 steel in different concentrations of HCl solutions containing H_2S at 90°C [J]. Corrosion
258 Science, 2011, 53 (5): 1715–1723.
259 [11] B. Hirschorn, M.E. Orazem, B. Tribollet, V. Vivier, I. Frateur, M. Musiani.
260 Determination of effective capacitance and film thickness from constant phase-element
261 parameters[J]. Electrochimica Acta, 2010, 55 (21):6218–6227.
262 [12] M.R. S. Abouzari, F. Berkemeier, G. Schmitz, D. Wilmer. On the physical interpretation
263 of constant phase elements, Solid State Ionics, 2009, 180 (14): 922–927.
264 [13] Y.X. Wang, W.M. Zhao, H. Ai, X.G. Zhou, T.M. Zhang. Effects of strain on the
265 corrosion behaviour of X80 steel[J]. Corrosion Science, 2011, 53(9): 2761–2766.
266 [14] M.C. Fatah, M.C. Ismail, B. Ari-Wahjoedi, K.A. Kumia. Effects of sulphide ion on the
267 corrosion behavior of X52 steel in a carbon dioxide environment at temperature 40℃[J].
268 Materials Chemistry & Physics, 2011, 127(1–2): 347–352.
269 [15] B.W.A. Sherar, I.M. Power, P.G. Keech, S. Mitlin, G. Southam, D.W. Shoesmith.
270 Characterizing the effect of carbon steel exposure in sulfide containing solutions to
271 microbially induced corrosion [J]. Corrosion Science, 2011, 53(3): 955–960.
272 [16] I. Betova, M. Bojinov, O. Hyöyvirta, T. Saario. Effect of sulphide on the corrosion
273 behaviour of AISI 316L stainless steel and its constituent elements in simulated Kraft
274 digester conditions[J]. Corrosion Science, 2010, 52(4): 1499–1507.

275 [17] B. Lin, R.G. Hu, C.Q. Ye, Y. Li, C.J. Lin. A study on the initiation of pitting corrosion
276 in carbon steel in chloride-containing media using scanning electrochemical probes[J].
277 Electrochimica Acta, 2010, 55(22): 6542–6545.